Multifunctional Hyperbolic Nanogroove Metasurface for Submolecular Detection

Li Jiang, Shuwen Zeng, Zhengji Xu, Qingling Ouyang, Dao-Hua Zhang, Peter Han Joo Chong, Philippe Coquet, Sailing He, and Ken-Tye Yong**

***M**etasurface serves as a promising plasmonic sensing platform for engineering the enhanced light–matter interactions. Here, a hyperbolic metasurface with the nanogroove structure in the subwavelength scale is designed. This metasurface is able to modify the wavefront and wavelength of surface plasmon wave with the variation of the nanogroove width or periodicity. At the specific optical frequency, surface plasmon polaritons are tightly confined and propagated with a diffraction-free feature due to the epsilon-near-zero effect. Most importantly, the groove hyperbolic metasurface can enhance the plasmonic sensing with an ultrahigh phase sensitivity of 30 373 deg RIU^{-1} and Goos–Hänchen shift sensitivity of 10.134 mm RIU^{-1}. The detection resolution for refractive index change of glycerol solution is achieved as 10^{-8} RIU based on the phase measurement. The detection limit of bovine serum albumin (BSA) molecule is measured as low as 0.1×10^{-18} M (1×10^{-19} mol L^{-1}), which corresponds to a submolecular detection level (0.13 BSA mm^{-2}). As for low-weight biotin molecule, the detection limit is estimated below 1×10^{-15} M (1×10^{-15} mol L^{-1}, 1300 biotin mm^{-2}). This enhanced plasmonic sensing performance is two orders of magnitude higher than those with current state-of-art plasmonic metamaterials and metasurfaces.*

Metasurfaces are engineered 2D artificial nanostructures to manipulate the propagation, reflection, refraction, and even photonic spin hall effect of the electromagnetic waves.[1–5] The patterning structures (i.e., scatterers or antennas) introduce local phase discontinuities to change the optical properties of propagating light.[6–11] The planarized metasurfaces can confine the light in the plane and these surface waves suffer low loss due to the ultrathin thickness in the

L. Jiang, Dr. S. Zeng, Dr. Z. Xu, Q. Ouyang, Prof. D.-H. Zhang, Prof. K.-T. Yong
School of Electrical and Electronic Engineering
Nanyang Technological University
639798, Singapore
E-mail: ktyong@ntu.edu.sg

L. Jiang, Prof. S. He
State Key Laboratory of Modern Optical Instrumentation
Centre for Optical and Electromagnetics Research
JORCEP (Sino-Swedish Joint Research Center of Photonics)
Zhejiang University
Hangzhou 310058, China
E-mail: sailing@kth.se

DOI: 10.1002/smll.201700600

L. Jiang, Dr. S. Zeng, Q. Ouyang, Prof. P. Coquet
CINTRA CNRS/NTU/THALES
UMI 3288, Research Techno Plaza
50 Nanyang Drive, Border X Block 637553, Singapore

Prof. P. H. J. Chong
School of Engineering
Computer and Mathematical Sciences
Auckland University of Technology
Auckland 1142, New Zealand

Prof. P. Coquet
Institut d'Electronique
de Microélectronique et de Nanotechnologie (IEMN)
CNRS UMR 8520 – Université de Lille 1
Villeneuve d'Ascq 59650, France

subwavelength scale.[5,12] Hyperbolic metasurfaces, uniaxial media, can be employed to control near-field waves such as surface plasmon polaritons (SPP).[13–16] Surface plasmons are collective conduction band electrons oscillations on the metal–dielectric interface and have a great potential application in the plasmonic sensing.[17–20] The metallic groove nanostructures as a newly developed type of 1D nanowire arrays were predicted to be able to confine the surface plasmon waves tightly to the metal surface.[16] The shape of the equal-frequency contours of surface plasmon polaritons changes from elliptical to hyperbolic with respect to the optical frequency. Normal diffraction and anomalous diffraction of surface plasmons correspond, respectively, to the elliptical and hyperbolic contours. Epsilon-near-zero effect[21] and epsilon-near-pole resonance[22] are special regimes at special frequency. The metasurfaces with epsilon-near-zero regime has the significant property of diffraction free. In this special case, the propagation of the surface plasmons is confined in the nondivergent direction.[16] Therefore, with extreme topological transitions, metallic nanogroove metasurface can provide unprecedented control of surface plasmon polaritons propagation.[14]

More importantly, the nanogroove hyperbolic metasurface also provides a plasmonic platform for engineering the enhanced light–matter interactions. It has been demonstrated that the plasmon polaritons can be confined on the top of the metallic groove ridge.[23] This confinement is achieved as the effective refractive index of the ridge plasmon is larger than that of the continuous metallic film.[16] The strong confinement of surface plasmons on the groove ridge creates the enhancement of the local electric field. Also, the profile of the groove nanostructure increases the sensing surface area and thus more biomolecules can be trapped into the groove grid. The surface plasmons on the hyperbolic metasurface can accumulate the abrupt phase change much sharper than the continuous metallic film for the hyperbolic dispersion.[24] Moreover, the nanogroove hyperbolic metasurface is superior to the conventional 3D plasmonic sensing structures due to the reduced propagation loss, ultrathin thickness, low cost planar fabrication, and facile integration with other optoelectronic components. Therefore, the nanogroove hyperbolic metasurface has the potential for the detection of low weight biomolecules (i.e., viruses, DNA, and hormones) with the enhanced plasmonic sensing performances.

In this paper, we have designed a hyperbolic metasurface with metallic nanogroove structure. This nanogroove metasurface provides multifunctions as: (i) to control and manipulate surface plasmon polaritons and modify the wavelength of the surface plasmon waves. The effective permittivity of the metasurface is tunable with the variation of the width and periodicity of the nanogroove structure; (ii) to be able to obtain hyperbolic dispersion by tuning the light wavelength in the visible region. As the width and periodicity are fixed at 30 and 150 nm, the nanogroove metasurface shows hyperbolic dispersion at optical wavelengths above 500 nm; (iii) the surface plasmon polaritons can propagate along a nondivergent direction as the permittivity of metasurface is in the epsilon-near-zero regime. For the groove nanostructure with the width of 30 nm and the periodicity of 150 nm, the effective refractive index of the metasurface is equal to zero at the ultraviolet wavelength; (iv) ultrahigh sensitivity for plasmonic detection was achieved. Even tiny perturbation of the surroundings will lead to a pronounced phase change and related Goos–Hänchen (GH) shift (higher order derivation of phase) of the propagating surface waves.

We have experimentally investigated the properties of the groove hyperbolic nanostructure for surface plasmon sensing of the glycerol solutions with different refractive index and the binding interactions of bovine serum albumin molecules with different concentrations. Differential phase change and GH shift between transverse magnetic (TM)-polarized light and transverse electric (TE)-polarized light are measured to evaluate the sensing performances of the nanogroove hyperbolic metasurface. The sensitivity of differential GH shift is up to 10.134 mm RIU^{-1}, which is more than two orders of magnitude better than the current 3D hyperbolic metamaterials comprised by multilayer gold films and aluminum dioxide.[25] The detection limit of the hyperbolic metasurface is as low as 0.1×10^{-18} M (1×10^{-19} mol L^{-1}) for bovine serum albumin solutions and 1×10^{-15} M (1×10^{-15} mol L^{-1}) for biotin solutions, which corresponds to a detection limit of 0.13 bovine serum albumin molecules (0.13 BSA mm^{-2}) and 1300 biotin molecules (1300 biotin mm^{-2}) in the illuminated area.

The designed hyperbolic metasurface with the groove nanostructure was carved into the metal with the width w and the periodicity p. **Figure 1** presents the scanning electron microscope (SEM) image of the nanogroove hyperbolic metasurface. The hyperbolic metasurface comprises six patches of nanogroove arrays and each patch contains 5 × 5 subwavelength groove nanostructures. The periodicity and width of the groove nanostructure are 150 and 30 nm.

Here, we calculated their optical parameters based on the dispersion relation of the anisotropic metasurface below:

$$\frac{k_x^2}{\varepsilon_y} + \frac{k_y^2}{\varepsilon_x} = \frac{w^2}{c^2} \tag{1}$$

w is the angular frequency of the radiation and c is the velocity of light in the vacuum.

The electric permittivity tensor of the uniaxial groove nanostructure can be considered as:

$$\overleftrightarrow{\varepsilon} = \begin{pmatrix} \varepsilon_x & 0 \\ 0 & \varepsilon_y \end{pmatrix} \tag{2}$$

The nanogroove hyperbolic metasurface is defined as a novel type of 1D nanowire arrays.[26,27] The effective medium theory gives the calculations of the effective permittivity in the x-direction (ε_x) and y-direction (ε_y) of the groove nanostructure:

$$\varepsilon_x = \frac{(1+\rho)\varepsilon_m\varepsilon_d + (1-\rho)\varepsilon_d^2}{(1+\rho)\varepsilon_d + (1-\rho)\varepsilon_m} \tag{3}$$

$$\varepsilon_y = \rho\varepsilon_m + (1-\rho)\varepsilon_d \tag{4}$$

With $\rho = (p - w)/p$, p and w represent the periodicity and width of the groove nanostructure, respectively.

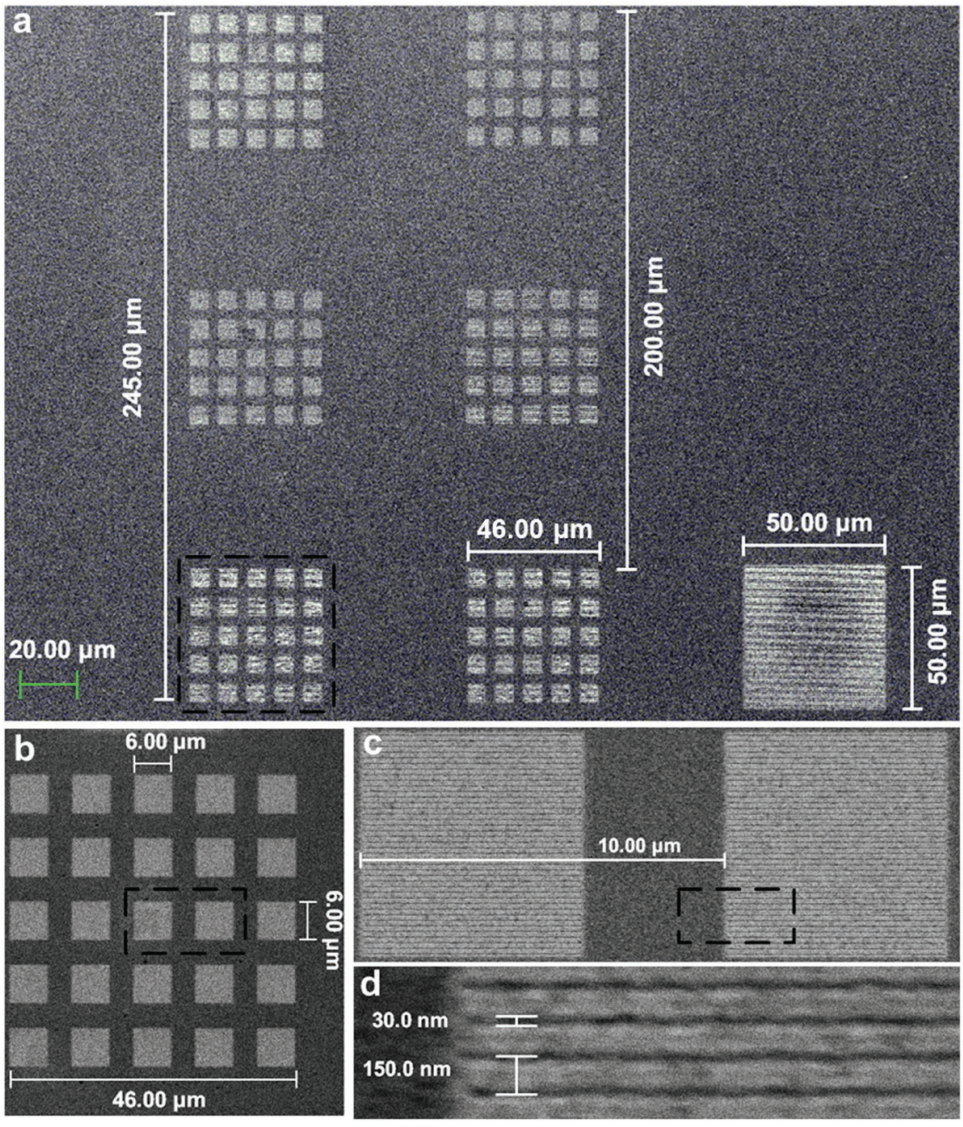

Figure 1. SEM images of the nanogroove hyperbolic metasurface. a) The distribution of the six patches of nanogroove arrays and the coupling grating structure. b) The enlarged view of one patch of nanogroove arrays. Each patch consists of 5 × 5 groove nanostructures. c) The enlarged view of the two adjacent groove nanostructures. d) The detailed view of the groove nanostructure with the width of 30 nm and the periodicity of 150 nm.

Both the effective permittivity in the *x*-direction and *y*-direction are closely associated with the parameters of width and periodicity (Figure S1, Supporting Information). Finite element analysis method (COMSOL Multiphysics 5.0) was employed to investigate the modification process of surface plasmon waves by the nanogroove metasurface. We first fixed the wavelength and the periodicity as 150 nm and tuned the width from 10 to 60 nm. **Figure 2**a shows that propagation of the surface plasmon waves along the groove nanostructures with the different widths but the same periodicity. The distances between two constructive interference fringes of surface plasmon waves are indicated by the dashed straight lines. The fringe space was increased with the broadening widths. To further investigate the plasmon propagation at the nanogroove interface, near-field scanning optical microscopy (NSOM) was used to characterize their excited electric field distributions (Figure 2b). Linearly polarized light from He–Ne laser was normally incident into the grating to couple the light from the free space to the in-plane surface plasmon waves (Figure S2, Supporting Information). The grating was used to couple the light to SPP and this coupling grating is shown in right corner in Figure 1a. The size of the grating is 50 × 50 μm^2. The NSOM tip coated with aluminum was placed 10 nm above the nanogroove metasurface (p = 150 nm and w = 30 nm). The collected near-field electric information was amplified by a photomultiplier tube (PMT). The NSOM results demonstrate that the nanogroove metasurface can directly manipulate the surface plasmon waves coupled from the gratings. The constructive and destructive interferences are, respectively, indicated by the bright and dark fringes.

As the permittivities of metal and dielectric vary at different wavelengths, the effective permittivity of the nanogroove metasurface is wavelength-dependent as well. Figure 2c,d is the calculation results of the real and imaginary part of the permittivities for the nanogroove metasurface in the *x*- and *y*-directions, respectively. The effective permittivity

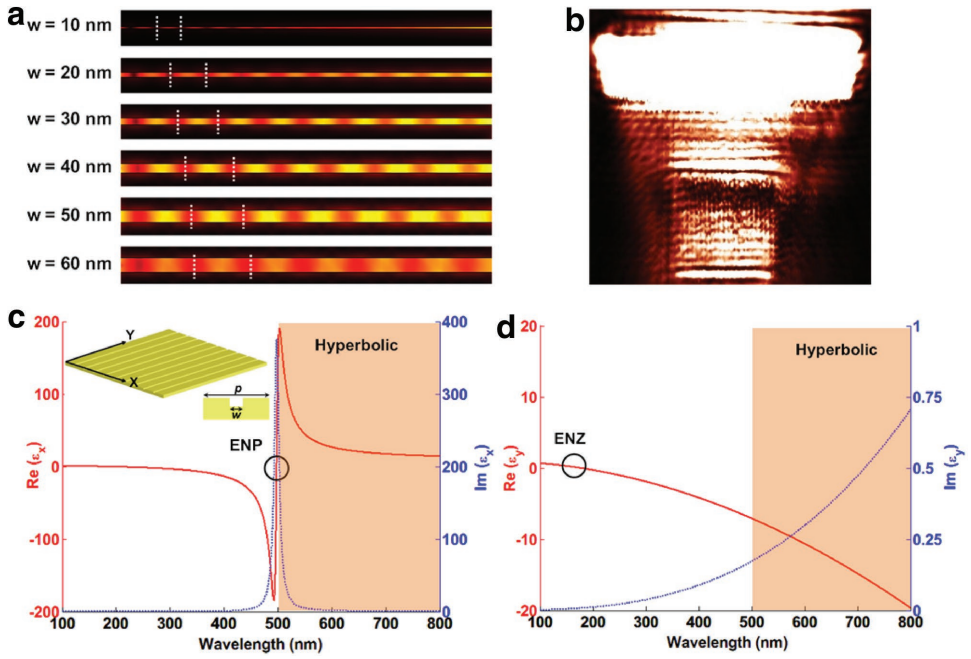

Figure 2. The manipulation of surface plasmon waves propagation by the nanogroove metasurface. a) Simulated electric field distributions of the surface plasmon polaritons on the groove nanostructure with the same periodicities but different widths. b) Measured near-field intensity distribution of metasurface. c) The electric permittivity of the nanogroove metasurface in the *x*-direction. d) The electric permittivity of the nanogroove metasurface in the *y*-direction.

of gold was calculated by the Drude–Sommerfeld model with interband absorption contributions. In the *y*-direction, the real part of the electric permittivity gradually decreases from 0.6675 to −19.6167 as the wavelengths change from 100 to 800 nm. The epsilon-near-zero (ENZ) effect occurs at the ultraviolet wavelength of 176 nm. Due to the Drude plasma frequency, the ENZ effect always exists in the direction of the free electron motion. In this case, the effective refractive index of the groove nanostructure is zero and the propagation of surface plasmon waves is tightly confined to this direction with a diffraction-free feature. In the *x*-direction, epsilon-near-pole (ENP) resonance can be excited at the visible wavelength of 500 nm. The ENP resonance occurs in the direction of noncontinuous free electron motion and perpendicular to the ridges of the groove nanostructures. Within the visible wavelength from 500 to 800 nm, surface plasmon waves show hyperbolic dispersion since the real part of the effective electric permittivity in the *x*-direction is positive while that in the *y*-direction is negative (Figure S3, Supporting Information).

Because the effective permittivity of the plasmon mode on the ridge of the groove is larger than that on the continuous metallic–dielectric interface, the surface plasmon waves are totally confined on the top of the groove ridges. The perturbations of the surroundings will cause the changes in the optical properties of the surface plasmon waves. Based on this specific performance, the nanogroove hyperbolic metasurface can be employed into the sensing application field. We use a prism coupling method to excite the surface plasmon waves on the nanogroove hyperbolic metasurface (**Figure 3**a). The phenomenon of surface plasmon resonance occurs when the wave vectors of the incident light couples well with that of the surface plasmon waves. This resonance resulted in a minimum reflectance (Figure S4b, Supporting Information), an abrupt phase change and an enhanced GH shift of the reflected light (Figure 3b). Here, GH shift is a small lateral shift of the TM-polarized light coupled and totally reflected from the nanogroove metasurface (**Figure 4**a). At the resonance condition, the electric field on the nanogroove metasurface is also strongly enhanced (Figure 3a and Figure S5 (Supporting Information)). The resonance angle and the enhancement of the electric field are shown to be associated with the parameter of groove width (Figure S6, Supporting Information). We also have experimentally demonstrated that the resonance angle for nanogroove metasurface differs from that for continuous gold thin film (Figure S4, Supporting Information), which is due to the difference in effective permittivity of metallic sensing surface.

To calibrate the sensing performance of the nanogroove metasurface, glycerol solutions with different concentrations were flowed to the nanogroove metasurface, which affected the resonance condition between the incident light and the surface plasmon polaritons. Two optical setups were employed to measure the differential phase change and GH shift of the reflected light (Figures S7 and S8, Supporting Information). Figure 3c reveals that the differential phase increases and gradually saturates with the increasing of the refractive index of the glycerol solutions. The linear change of the differential phase is up to 36.448° corresponding to the refractive index from 1.3326 to 1.3338. The sensitivity of the differential phase is up to 30 373 deg RIU^{-1}, which is almost five times higher than that of conventional continuous gold thin film (Figure S9, Supporting Information). The phase detection resolution is achieved as low as 10^{-8} RIU with the

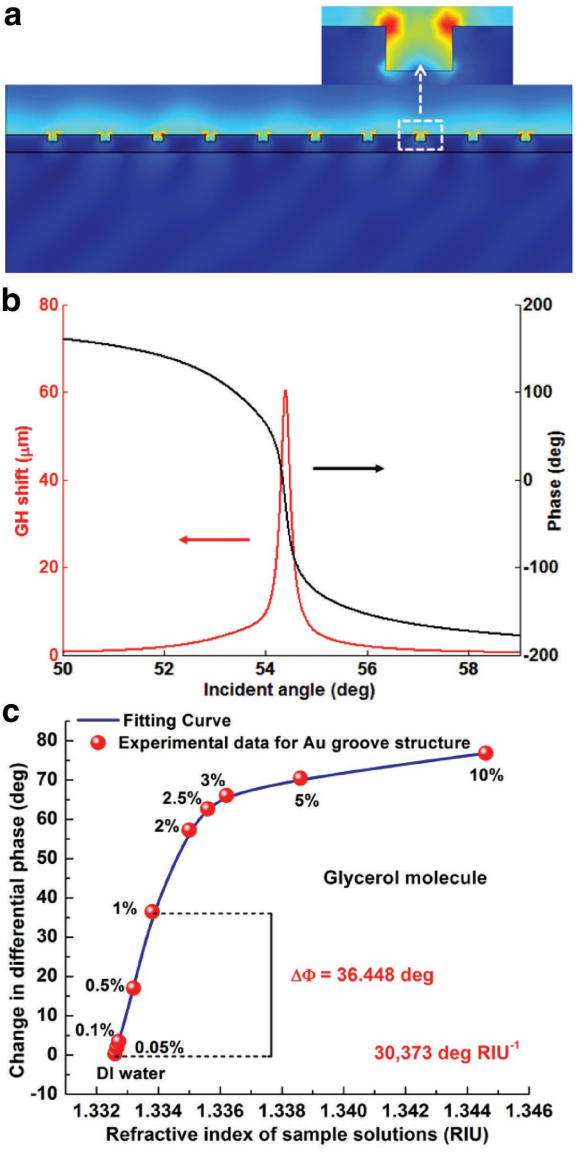

Figure 3. The strong light–matter interactions of the nanogroove hyperbolic metasurface. a) The electric filed distribution showing the enhancement on the nanogroove surface at the resonance condition. b) The simulation data of GH shift and phase with respect to the incident angle. The largest GH shift corresponding to the sharpest phase change at the surface plasmon resonance. c) The change in differential phase of the reflected light with the injection of the glycerol solution with different concentrations.

system noise of 0.001°. As shown in Figure 4b, the largest GH shift is up to 59.9 μm, which corresponds to the sample solution of deionized (DI) water under the surface plasmon resonance condition. Then the differential GH shift changes linearly (as shown in the inset of Figure 4b) and gradually saturates with the increasing of the glycerol concentration. The sensitivity of the differential GH shift is up to 10.134 mm RIU^{-1}, which is more than two orders of magnitude better than that with the multilayer hyperbolic metamaterials (30 μm RIU^{-1})[25] and other plasmonic metamaterials[28] either with the gold nanodots or graphene crystal.

These plasmonic sensing characteristics (i.e., phase change and GH shift) are mainly dependent on the near-field light–matter interactions. The excited light, coupled as surface plasmon polaritons, are totally confined in the plane of nanogroove metasurface due to the extreme anisotropy hyperbolic dispersion. Additionally, the contribution of the local density of states could be considered more significant than that of the photonic density of states due to the subwavelength structures of the periodic nanogrooves. This periodic patterning could also cause the formation of the surface plasmon photonic band gap where the density of the surface plasmon states is high at the edges. The tight confinement of the surface plasmons in the sensing plane and the increased local density of states on the groove ridges facilitate the enhancement of the electric field distributions and activities.

Through our designed hyperbolic metasurface, the interference between the excited light and surface plasmons waves propagating in the same direction could accumulate a relative phase lag. The minimum intensity of the reflected light from the nanogroove metasurface corresponds to the constructive interference. Near-zero reflection (darkness point) can be achieved by selecting the coupling angle, which corresponds to a singular phase. This phase change accumulates more sharply at the darker point of the reflected light. Due to the effective permittivity of the hyperbolic metasurface, a perfect interference could occur by tuning the nanogroove parameters. The effective permittivity of the metallic metasurface is also defined by the Drude model. The value associates tightly with the plasma frequency and the damping constant. For the nanogroove hyperbolic metasurface, the effective damping constant of the metallic surface is likely higher than that of the continuous metallic film due to the surface scattering and grain boundary effects. This higher damping constant also attributes to a darker reflection. Therefore, the designed hyperbolic metasurface could support the perfect absorption and the enhanced phase change as well as GH shift due to the constructive interference and increased damping constant. In brief, the more energy of the incident light is transferred to afford the oscillations of collective electrons, and the larger resonant electric field is enhanced. The enhancement of the electric field directly determines the maximum sensitivity for medium dielectric change.

This designed nanogroove hyperbolic metasurface was then employed to monitor the binding interactions of bovine serum albumin (BSA, 67 kDa) molecules in extremely diluted solutions. BSA is widely used to determine the quantity of other proteins through Bradford protein assay. BSA molecules were directly attached to the nanogroove metasurface through physisorption interactions.[29,30] As depicted in Figure 4c, DI water was first flowed to the nanogroove metasurface for 5 min to rinse the sensing surface and be set as a sensing baseline. Then, the BSA sample solution was pumped to the sensing surface at a constant speed by the syringe for 20 min. Since surface plasmon resonance effect was excited in this case, even tiny refractive index change on the metasurface due to the biomolecules binding would cause an observable GH shift. The change of differential GH shift showed an increase in the binding event of BSA molecules onto nanogroove metasurface from 5 to 15 min and gradually saturated with time. For the last step, DI water was injected for 5 min

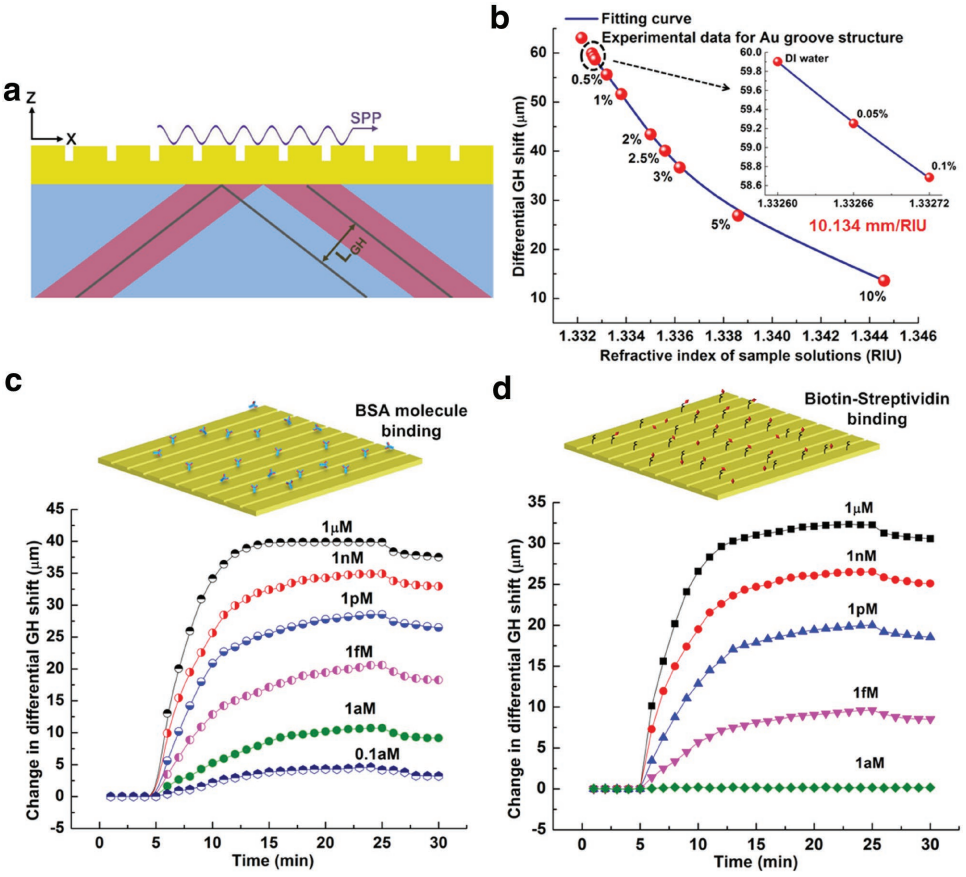

Figure 4. Plasmonic sensing performance of the nanogroove hyperbolic metasurface based on the measurement of the Goos–Hänchen shift. a) The schematic diagram of the enhanced GH shift. b) Differential GH shift with respect to the concentration of glycerol solutions. c) The binding interaction of bovine serum albumin molecules diluted from 0.1×10^{-18} to 1×10^{-6} M measured by the change in differential GH shift. d) Biotin with low molecular weight of 244 Da binding with the streptavidin molecules functionalized on the groove metasurface.

to flow away the unbounded BSA molecules, which resulted in a little decreased GH shift. The binding interactions of the BSA sample solutions with different concentrations of 0.1×10^{-18}, 1×10^{-18}, 1×10^{-15}, 1×10^{-12}, 1×10^{-9}, and 1×10^{-6} M were detected, respectively. The results indicated that BSA sample solutions with higher concentrations would cause larger differential GH shift due to more BSA molecules in the sample solutions. Based on the experimental results, we demonstrated that the detection limit of the BSA sample solutions was below 0.1×10^{-18} M, which corresponds to only 0.13 BSA molecules in the illuminated area (0.13 BSA mm^{-2}) (details for estimation of the detection limit, see Section S3.1 in the Supporting Information).

In order to investigate the detection ability of the nanogroove metasurface, we also carried out the experimental measurements on the low-weight biotin molecules (244 Da) using the standard biotin–streptavidin model. The 1×10^{-6} M streptavidin molecules were functionalized on the nanogroove metasurface through physisorption forces[31,32] for 10 min (Figure S10, Supporting Information), which was employed to capture the biotin molecules.[25] The phosphate buffered saline buffer was flowed as the baseline and then biotin molecules were injected into the reaction chamber with diluted solutions (Figure 4d). The change in differential GH shift demonstrated the kinetic process for BSA molecules binding with streptavidin molecules. The results indicated that the detection limit of biotin molecules was below 1×10^{-15} M based on the nanogroove metasurface, while the interaction between the 1×10^{-18} M biotin and the streptavidin showed no signal response in the GH shift (details for estimation of the detection limit, see Section S3.2 in the Supporting Information). The binding event of biotin molecules onto the nanogroove metasurface without functionalization of streptavidin molecules was also monitored (Figure S11, Supporting Information), which further demonstrated the repeatability of the nanogroove metasurface. The smaller biomolecule corresponded to a worse detection limit.

Our designed nanogroove hyperbolic metasurface presents strong light–matter interactions that can achieve submolecule detection with ultrahigh sensitivity. The propagations of the surface plasmon waves can be controlled and manipulated by the groove nanostructures. The electric field on the sensing surface is significantly enhanced due to the highly confined surface plasmons in the plane and the increased local density of states on the groove ridge. The perfect absorption can be achieved due to the constructive interference and increased damping constant of the hyperbolic metasurface. By tuning the optical frequency, surface plasmon waves can be tightly confined and propagating in a diffraction-free direction induced by the zero refractive index.

These significant performances of the nanogroove metasurface would allow the creation of on-chip multifunctional photonic and optoelectronic devices for biosensing, imaging, and quantum communication.

Experimental Section

Fabrication of the Hyperbolic Nanogroove Structure: The groove nanostructure was fabricated on the gold substrate using focused ion beam (FIB) from Carl Zeiss AURIGA crossbeam (FIB-SEM) workstation. The ion source was Gallium (Ga) at 30 keV beam energy. For milling the groove patterns, 20 pA beam current was chosen with minimum spot size of 13 nm. In addition, the milling of the grating structure was carried out at 120 pA beam current (for its fast operation).

Characterization of the Excited Electric Field Distributions on the Nanogroove Surface: NSOM was used to characterize the excited electric field distributions and to demonstrate that the nanogroove structure could propagate the surface plasmon polaritons. The light from He–Ne laser (Thorlabs, 0.5 mm beam width, 20 mW power, $\lambda = 632.8$ nm) was TM polarized and focused onto the grating from the bottom of the sample substrate at normal incidence by 10× objective lens (Olympus UPlanFLN NA = 0.3). The NT-MDT NSOM system was mounted with an inverted microscope (Olympus IX71) equipped with a PMT for signal detection and amplification. The aluminum-coated NSOM probe tip was less than 100 nm in diameter and positioned ≈10 nm from the sample substrate. This distance was achieved by shear-force feedback mechanism to perform the precise control. The fiber tip was glued with a tuning fork, which was mounted on a piezoelectric tube dithering and scanning parallel to the sample surface. The vibration of the tuning fork changes rapidly as it approaches the sample surface perpendicularly at distances of about tens of nanometers. The resonance frequency was chosen 33 KHz for quartz crystal tuning fork. The tip could be maintained at a relatively stable distance during the scanning.

Phase Measurement: The light from the He–Ne laser was incident into the polarized beam splitter and then was separated into TM-polarized light and TE-polarized light. The beam of TM-polarized light arrived at the nanogroove hyperbolic metasurface which was coupled with a SF11 prism on a translation stage. A phenomenon of surface plasmon resonance would take place by rotating the stage and TM-polarized light was fixed at the surface plasmon resonance angle. The sample solutions were flowed to the nanogroove metasurface with a syringe, which would affect the resonance between the incident TM-polarized light and excited surface plasmon polaritons. The beam of TE-polarized light went through the vibrating galvo-mirror (Thorlabs, GVS001) controlled by a signal generator. The phase of TE-polarized light was modulated due to the optical path difference. The reflected TM-polarized light from the coupling prism and TE-polarized light interfered after going through a polarized beam splitter and a polarizer. The data acquisition card (NI PCI-6115) was used to collect the interference intensity with the sampling rate of 100 kHz. Because only TM-polarized light could excite the surface plasmon resonance, only the phase of TM-polarized light carried the information of the sample solutions. The differential phase between TM-polarized light and TE-polarized light could be extracted through Matlab processing, which could eliminate the noise of the system.

Goos–Hänchen Shift Measurement: The surface plasmon resonance effect could enhance the GH shift of TM-polarized light. Therefore, differential GH shift between TM-polarized light and TE-polarized light could be regarded as an optical characteristic carrying the information of the sample solutions. The light from the He–Ne laser was separated into TM-polarized light and TE-polarized light by a polarized beam splitter. An optical chopper was placed to confirm that only one beam of TM-polarized light and TE-polarized light could go through the nanogroove hyperbolic metasurface coupled by the SF11 prism. The surface plasmon resonance angle was fixed by rotating the translation stage. The position of the reflected TM-polarized light and TE-polarized light could be detected by a lateral position sensor (Thorlabs, PDP90A). The differential GH shift could be obtained after Matlab processing procedures.

Supporting Information

Supporting Information is available from the Wiley Online Library or from the author.

Acknowledgements

*L.J., S.Z., and Z.X. contributed equally to this work. This work was prepared with support from the Singapore Ministry of Education (Grants Tier 2 MOE2010-T2-2-010 (M4020020.040 ARC2/11) and Tier 1 M4010360.040 RG29/10), the NTU-NHG Innovation Collaboration Grant (M4061202.040), the NTU–A*STAR Silicon Technologies, Centre of Excellence, under the program Grant No. 11235100003, and the School of Electrical and Electronic Engineering at the NTU.*

Conflict of Interest

The authors declare no conflict of interest.

[1] A. V. Kildishev, A. Boltasseva, V. M. Shalaev, *Science* **2013**, *339*, 1232009.
[2] D. Lin, E. Hasman, M. L. Brongersma, *Science* **2014**, *345*, 298.
[3] X. Yin, Z. Ye, J. Rho, Y. Wang, X. Zhang, *Science* **2013**, *339*, 1405.
[4] F. Aieta, M. A. Kats, P. Genevet, F. Capasso, *Science* **2015**, *347*, 1342.
[5] A. A. High, R. C. Devlin, A. Dibos, M. Polking, D. S. Wild, J. Perczel, N. P. de Leon, M. D. Lukin, H. Park, *Nature* **2015**, *522*, 192.
[6] N. Yu, P. Genevet, M. A. Kats, F. Aieta, J. P. Tetienne, F. Capasso, Z. Gaburro, *Science* **2011**, *334*, 333.
[7] F. J. Rodríguez-Fortuño, G. Marino, P. Ginzburg, D. O'Connor, A. Martínez, G. A. Wurtz, A. V. Zayats, *Science* **2013**, *340*, 328.
[8] N. Yu, F. Capasso, *Nat. Mater.* **2014**, *13*, 139.
[9] F. Ding, Z. Wang, S. He, V. M. Shalaev, A. V. Kildishev, *ACS Nano* **2015**, *9*, 4111.
[10] Z. Li, E. Palacios, S. Butun, K. Aydin, *Nano Lett.* **2015**, *15*, 1615.

[11] J. Lin, J. P. B. Mueller, Q. Wang, G. Yuan, N. Antoniou, X. C. Yuan, F. Capasso, *Science* **2013**, *340*, 331.
[12] S. Sun, Q. He, S. Xiao, Q. Xu, X. Lin, L. Zhou, *Nat. Mater.* **2012**, *11*, 426.
[13] G. Bartal, *Nature* **2015**, *522*, 160.
[14] J. S. Gomez-Diaz, M. Tymchenko, A. Alù, *Phys. Rev. Lett.* **2015**, *114*, 233901.
[15] E. Yoxall, M. Schnell, A. Y. Nikitin, O. Txoperena, A. Woessner, M. B. Lundeberg, F. Casanova, L. E. Hueso, F. H. L. Koppens, R. Hillenbrand, *Nat. Photonics* **2015**, *9*, 674.
[16] Y. Liu, X. Zhang, *Appl. Phys. Lett.* **2013**, *103*, 141101.
[17] S. Zeng, K. V. Sreekanth, J. Shang, T. Yu, C. K. Chen, F. Yin, D. Baillargeat, P. Coquet, H. P. Ho, A. V. Kabashin, K. T. Yong, *Adv. Mater.* **2015**, *27*, 6163.
[18] S. Zeng, D. Baillargeat, H. P. Ho, K. T. Yong, *Chem. Soc. Rev.* **2014**, *43*, 3426.
[19] J. N. Anker, W. P. Hall, O. Lyandres, N. C. Shah, J. Zhao, R. P. V. Duyne, *Nat. Mater.* **2008**, *7*, 442.
[20] M. E. Stewart, C. R. Anderton, L. B. Thompson, J. Maria, S. K. Gray, J. A. Rogers, R. G. Nuzzo, *Chem. Rev.* **2008**, *108*, 494.
[21] R. Maas, J. Parsons, N. Engheta, A. Polman, *Nat. Photonics* **2013**, *7*, 907.
[22] Z. Jacob, *Nat. Mater.* **2014**, *13*, 1081.
[23] E. J. R. Vesseur, R. de Waele, H. J. Lezec, H. A. Atwater, F. J. G. de Abajo, A. Polman, *Appl. Phys. Lett.* **2008**, *92*, 083110.
[24] K. Yao, Y. Liu, *Nanotechnol. Rev.* **2014**, *3*, 177.
[25] K. V. Sreekanth, Y. Alapan, M. Elkabbash, E. Ilker, M. Hinczewski, U. A. Gurkan, A. D. Luca, G. Strangi, *Nat. Mater.* **2016**, *15*, 621.
[26] P. Shekhar, J. Atkinson, Z. Jacob, *Nano Convergence* **2014**, *1*, 1.
[27] Z. Xu, T. Li, D.-H. Zhang, C. Yan, D. Li, L. Y. M. Tobing, F. Qin, Y. Wang, X. Shen, T. Yu, *Appl. Phys. Express* **2014**, *7*, 052001.
[28] V. G. Kravets, F. Schedin, R. Jalil, L. Britnell, R. V. Gorbachev, D. C. B. Thackray, K. S. Novoselov, A. K. Geim, A. V. Kabashin, A. N. Grigorenko, *Nat. Mater.* **2013**, *12*, 304.
[29] R. S. Moirangthem, Y. C. Chang, S. H. Hsu, P. K. Wei, *Biosens. Bioelectron.* **2010**, *25*, 2633.
[30] Y. Liu, R. Zhong, P. Zhang, Y. Ma, X. Yun, P. Gong, J. Wei, X. Zhao, F. Zhang, *ACS Appl. Mater. Interfaces* **2016**, *8*, 2478.
[31] E. Ouellet, C. Lausted, T. Lin, C. W. T. Yang, L. Hood, E. T. Lagally, *Lab Chip* **2010**, *10*, 581.
[32] D. Kim, A. E. Herr, *Biomicrofluidics* **2013**, *7*, 041501.

Received: February 22, 2017
Revised: April 2, 2017
Published online: June 8, 2017

